Robust Adaptive Optics Systems for Vision Science

Burns, SA[1], de Castro, A[1], Sawides, L[1], Luo, T[1], Sapoznik, K[1].

[1]Indiana University School of Optometry, 800 E. Atwater Ave, Bloomington, IN 47405

ABSTRACT

Adaptive Optics (AO) is of growing importance for understanding the impact of retinal and systemic diseases on the retina. While AO retinal imaging in healthy eyes is now routine, AO imaging in older eyes and eyes with optical changes to the anterior eye can be difficult and requires a control and an imaging system that is resilient when there is scattering and occlusion from the cornea and lens, as well as in the presence of irregular and small pupils. Our AO retinal imaging system combines evaluation of local image quality of the pupil, with spatially programmable detection. The wavefront control system uses a woofer tweeter approach, combining an electromagnetic mirror and a MEMS mirror and a single Shack Hartmann sensor. The SH sensor samples an 8 mm exit pupil and the subject is aligned to a region within this larger system pupil using a chin and forehead rest. A spot quality metric is calculated in real time for each lenslet. Individual lenslets that do not meet the quality metric are eliminated from the processing. Mirror shapes are smoothed outside the region of wavefront control when pupils are small. The system allows imaging even with smaller irregular pupils, however because the depth of field increases under these conditions, sectioning performance decreases. A retinal conjugate micro-mirror array selectively directs mid-range scatter to additional detectors. This improves detection of retinal capillaries even when the confocal image has poorer image quality that includes both photoreceptors and blood vessels.

Keywords: Adaptive Optics, Ophthalmic Imaging, Retinal Imaging, Confocal Imaging, Optics, Retina.

1. INTRODUCTION

Adaptive optics (AO) retinal imaging is of increasing importance in understanding the impact of retinal and systemic diseases. With the development of dark field techniques the Adaptive Optics Scanning Laser Ophthalmoscopes (AOSLO) have become a tool that can provide retinal imaging of multiple cellular and even subcellular features. There are a number of challenges that can make this imaging difficult in a broad clinical population. These limitations arise from a number of sources. First, patients do not have uniformly large clear pupils. Additionally, in the aged population cataracts and intraocular lenses (IOL's) are common, and due to lens capsule opacification pupils can be irregularly shaped. Second, while using a fixed offset aperture or knife-edge can allow multiply-scattered light to be used as a contrast mechanism, changing the imaging configuration based on local retinal features can be slow. Third, the size of the isoplanatic[1] patch in the retina can be small, especially in aging eyes, and thus, without using multi-conjugate adaptive optics[2, 3], adaptive optics works best for small field sizes. This limitation in turn means that the patient must actively fixate a moveable fixation target or the field must be moved. These movements can cause cyclotorsion, or if the field is moved it can distort with scanning angle. Finally, the patient's head also moves, and is often countered by the use of dental impressions or tight head restraints, making the imaging session less enjoyable for the patient.

Modern retinal imaging systems also provide a number of methods for generating contrast or unique information that are desirable in some retinal diseases. In the current work we wanted to apply AO to improving two particular forms of imaging. The first is based on using multiple scattering to generate contrast of scattering structures in the retina, and the second is to improve on the ability to measure rapid events in the retina. For the first, it has been recognized since the development of dark field microscopy that wider angle scattering can provide additional information on the scattering structures. In a typical confocal imaging system light is collected from the center of the point spread function (PSF). Light falling outside the center of the PSF is rejected by the confocal pinhole. In the retina, which is specialized to be highly transparent in healthy eyes, dark field techniques can be used to emphasize low contrast structures while suppressing the Fresnel reflection from abrupt index of refraction boundaries. Thus, a number of techniques have been developed to use multiply scattered light as a contrast mechanism for imaging the retina [4-9]. In these techniques, directly backscattered light is typically collected by a confocal aperture, or blocked if not desired, and light that is multiply scattered is collected using an offset aperture[10, 11] or a reflective knife edge which directs light into two detectors[12]. These techniques provide superb results, but can be limiting since there are strong anisotropies in the retinal scattering, particularly from oriented structures such as blood vessels[8]. Thus, in our new system we implemented a form of programmable array microscopy where we could vary the size, shape and orientation of the detection aperture[13], and direct light from

arbitrarily shaped regions of the PSF to two different detectors. The second specialization we developed is based on the observation made with the multiply scattered light imaging that red blood cells provide excellent scattering centers, and thus can be observed directly. This opens the possibility of in vivo tracking of individual red blood cells. The major limitation is that, depending on the velocity and arrangement of cells, a traditional progressive scan system could under sample the data. Thus we developed a two beam approach where at any instant two separate wavelengths are sampling slightly different regions of the retina. In our case, if we separate scans by a few 10's of lines, the same cell can be imaged twice in succession, with the time interval on the order of a few milliseconds, allowing us to accurately measure blood cell velocity over a range of speeds[14].

The current paper presents our approach to controlling the wavefront during patient imaging in a manner that allows rapid and reliable wavefront control under non-ideal situations that are encountered in real-life. We then present an optical system that incorporates this approach to wavefront control and also allows adaptive detection strategies and measurements of rapidly changing conditions, while providing more flexibility in adapting the system to the patient's unique needs.

2. METHODS

2.1 Optimizing Wavefront Control to respond to irregular pupils and head motions.

We developed improved wavefront control algorithms to deal with small, as well as irregular pupils which occur with treatment for posterior capsule opacification. The approach has also been designed to help control the abruptly changing wavefront [15, 16] which is common with intraocular lenses (IOL's). The problems in wavefront control in these situations arise from several sources, including errors in centroiding of Shack Hartmann (SH) spots and from practical aspects that arise from patient head and pupil movement. The centroiding errors often arise because light returning from the human retina, through the pupil, ideally represents a sharp image of the beacon light on the retina. However, the SH sensor has a very large depth of field, with each lenslet often having an f# on the order of 25-30. This means that the images contain not only the directly reflected image of the beacon, but also a more diffuse component that arises from multiple scattering[17] as well as from reflections from out of focus elements. The desirable, singly scattered component produces the image of the wavefront sensing beacon, and the multiply scattered light component, as well as reflections from the anterior eye, represents the broad surround of the PSF. Therefore in the human eye in order to find the local slope of the wavefront most algorithms implement a multi-step approach to determining the centroid of the beacon image. These enhance the accuracy by computing local centroids [18] which decreases the bias from the background light. However, even this multi-stage approach can be compromised if there are large artifacts, if a lenslet is only partially illuminated, or there are significant aberrations across the subaperture of a lenslet. These can occur relatively often while imaging patients. Small and irregular pupils can cause edges of the pupil to produce only partially illuminated pupil sub apertures, and these edges can move if the head moves even as little as 0.3 mm, making a fixed approach to remediating these motions difficult. In addition, the presence of IOLs, which are often smaller than the dilated pupil, can cause abrupt transitions of the wavefront across the pupil, as well as large reflection artifacts from the surface of the IOL. Figure 1 illustrates both the
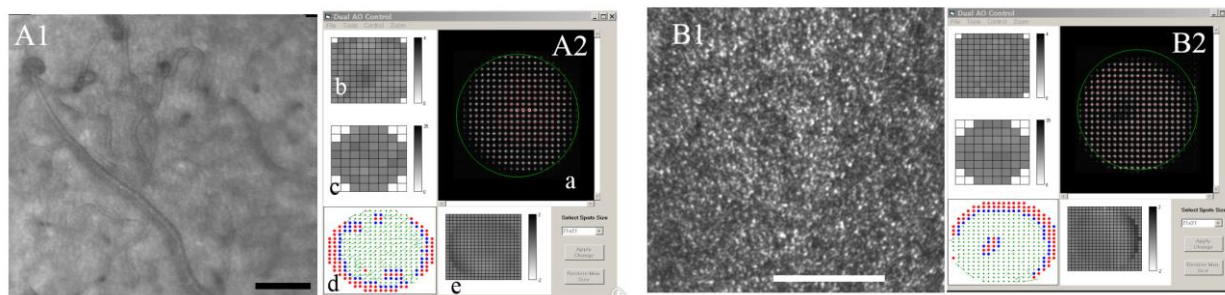

Figure 1. Examples of retinal images (A1 and B1) and wavefront control interface (A2 and B2). Subject A is a diabetic subject with an IOL. **A1**, retinal image using multiply scattered light showing capillary remodeling and small microaneurysm. **A2**, the wavefront control interfaces, showing the SH image (**A2a**), where the **green line** represents the edge of the system optical pupil and the spots represent the intensity distribution of spots on the CCD, but with strong signals of the 12 bit data set to red to allow dim pixels to be visualized. Along the left edge are the maps of current mirror deflections for the BMC mirror (**A2b**), Mirao mirror (**A2c**) and a colored vector map of current deflections for each lenslet (**A2d**). Color codes are described in the text. At the bottom is the residual wavefront error map (**A2e**). B1 and B2 show the same information for a subject with a small subcapsular cataract. Scale bars represent 100 μm.
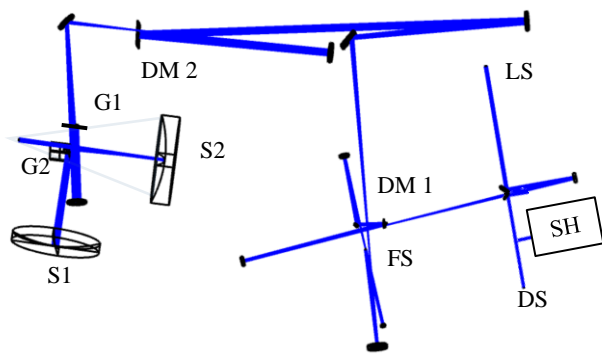
Figure 2. Schematic of the basic system design. An all reflective design is used, folded in 3 dimensions to allow cancellation of off-axis astigmatism. LS: Light Source Supercontinuum Laser (Fianium), SH: Shack Hartmann Sensor, FS, fast scan resonant scanner (15.8 kHz), DM1: deformable mirror 1, Boston Micromachines, 141 element mirror, DM2, deformable mirror 2, Mirao 52D, G1: Steering Galvo for horizontal positioning, G2, Steering Galvo for vertical positioning and slow scan. System design for 2.5 diopter myope at deformable mirror 2.

problem, as well as results for the wavefront control technique. Here we show both retinal images (A1 and B1) as well as the control interface (A2 and B2) for two patients. The SH images (top right of both A2 and B2) show that in these cases while the system pupil was 8 mm (represented by the green line), the patient did not dilate to this extent. A typical approach to handle this is to shrink the computational pupil[15]. The disadvantage of this approach is that the patient must be well stabilized relative to the system, since now there are relatively fewer interior samples for the Shack Hartmann (SH) sampling grid. However it is also clear that in these subjects the edges of the pupil return dimmer spots, presumably because they are not fully illuminated and if incorporated into the wavefront control calculations will cause errors in the wavefront slope calculation. Our approach is to compute a simple metric to represent the quality of the spot produced by each lenslet. This metric is the fraction of the total amount if light returning within the lenslet (by summing all pixels within the grid location of that lenslet) that is contributed by the center of the SH spot, typically roughly twice the size of Airy disc for the lenslet. When this metric is high, the spot is well formed and can present a robust estimate of the wavefront slope. When this metric is low, much of the light is coming from diffuse scatter, or out of focus structures (such as the cornea or an IOL). We then filter the lenslets with low metrics from the control matrix. In figure 1, spots which exceed the metric threshold, which can be set by the operator, are colored green, those that fail are colored red. Border spots are colored blue (see below). The algorithm then eliminates slopes determined from lenslets with low metrics and lenslets from the border between lenslets with high and low metrics from the computation. Next the desired mirror change is calculated not only from the good spots, but from a low pass filter of the slopes outside the border region. This helps to stabilize the mirror shape outside the control region, so that if the eye moves slightly, there is not an abrupt transition in the wavefront control.

2.2 Optical Design for wide field steering and montaging

We designed a new AOSLO that would provide both excellent image quality for a small field and allow the small imaging field to be moved without scan distortion over an approximately 30° field. When this is coupled with a programmable fixation system it allows imaging of the posterior pole of the eye over roughly 40° without auxiliary fixation points. The system was designed in ZEMAX and modeled using Solidworks and follows a fairly standard, all reflective design, using combinations of vertical and horizontal folding cancel off-axis astigmatism [19-22]. The front end of the system incorporates wide field scanning by incorporating two separate scanners, one for vertical deflections, and one for horizontal deflections. These scanners are located such that rather than operating at one focal length from the large field mirrors, they are closer to the center of curvature of the field mirrors, which decreases the induced astigmatism as the field is scanned. They are not located exactly at the 2f location to allow a slight tilt of the beams (to avoid blocking the beams, and to allow increased head and face clearance for subjects). The use of two galvanometers avoids some of the rotation of the imaging field which can arise when a single surface is rotated in two dimensions. The final design and the predicted optical performance are shown in Figure 2 and 3. This is a woofer tweeter design that combines the large stroke of an electromagnetic mirror (M2, Mirao 52 D, Imagine Eyes), with the high frequency low stroke capability of a MEMs mirror (M1, Multi-DM, Boston Micromachines, Cambridge, MA). Because we want to be able to use pupils up to 8 mm, but also function adequately for small pupils, the combination allows even relatively good control for small pupils, which in older eyes can have considerable aberrations.

2.3 Optimizing Beam delivery and Optical Detection:

The system uses two wavelengths, filter selectable from a supercontinuum laser (Fianium, NKT Photonics, Birkerod, Denmark), with wavelength separated at 800 nm. The longer wavelength can be tilted at the pupil plane to allow temporal offset imaging[14]. Light returning from the eye is separated by a dichroic filter, and the shorter wavelength light is
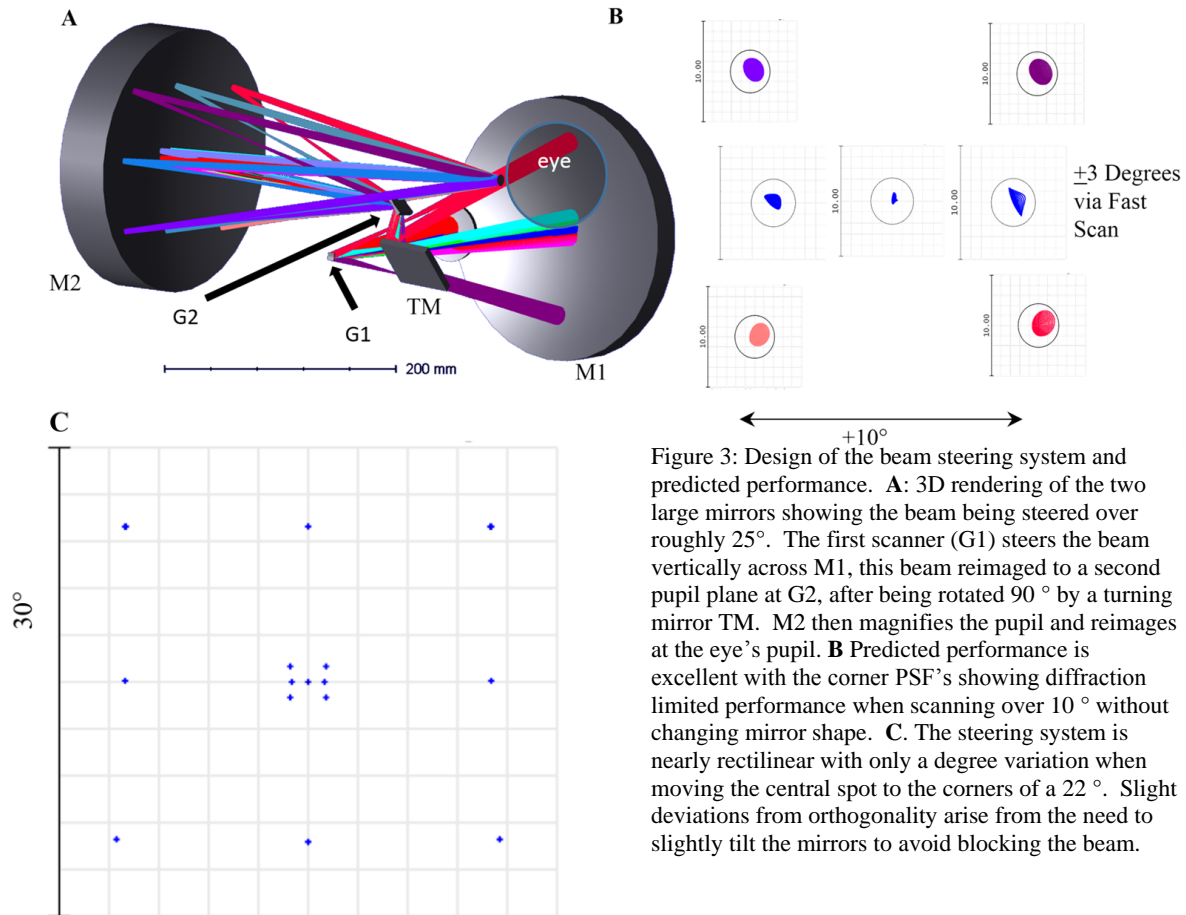
Figure 3: Design of the beam steering system and predicted performance. **A**: 3D rendering of the two large mirrors showing the beam being steered over roughly 25°. The first scanner (G1) steers the beam vertically across M1, this beam reimaged to a second pupil plane at G2, after being rotated 90 ° by a turning mirror TM. M2 then magnifies the pupil and reimages at the eye's pupil. **B** Predicted performance is excellent with the corner PSF's showing diffraction limited performance when scanning over 10 ° without changing mirror shape. **C**. The steering system is nearly rectilinear with only a degree variation when moving the central spot to the corners of a 22 °. Slight deviations from orthogonality arise from the need to slightly tilt the mirrors to avoid blocking the beam.

partially diverted to the SH sensor and the rest is imaged to a spatial mask located in a retinal conjugate plane. This mask is mounted on a computer controlled positioner and has a series of elliptical confocal aperture, ranging in size from ¼ of an Airy Disc to 20x an Airy disk diameter. The elliptical shape is used since the mask is located at a slight angle to the illuminating light (Figure 4), and light that does not go through the apertures is reflected and re-imaged onto the surface of a MEMS digital micro-mirror device (DLP6500, Texas Instruments, Dallas, TX). The actual design used paired lenses three element lenses (Thorlabs) to relay the image in order to accurately re-image the PSF onto the DMD surface. The individual MEMs mirror elements are programmed via Matlab (The Mathworks, Natick, MA, USA). Mirrors in the "on" state deflect light to the "on" detector, and those in the "off" state deflect light to the off detector. All detectors are based on APD chips (APD, Pacer C30659-90), together with custom amplifier and temperature controllers.

3. RESULTS

3.1 Wavefront Control:

The AO control algorithm is robust and allows imaging of relatively "difficult" eyes. Figure1 shows our SH image and a corresponding retinal image of a subject with an IOL (left) and an early cataract (right). Although the image quality metric is relatively simple, it successfully detects the edges of the pupil and regions where there quality of spots is low due to the transition from pupil areas overlying the IOL and areas where the IOL is not present (A2). It also correctly can decrease the influence of small cataracts. While image quality for these difficult cases is clearly not as good as would be achieved with full 8 mm pupils and clear optics, it is acceptable to make measurements such as vascular dimension (A1) or cone density (B1). In terms of usability, this algorithm also has decreased the pressure on keeping the subject absolutely still, since small displacements of the pupil within the system pupil are easily accommodated.

3.2 Optical Performance and Beam Steering

Physical constraints, such as mounting hardware for the slow scan galvanometer, restricted actual beam steering in the inferior visual field to roughly $+14°$ to $-8°$ vertical extent in the right left visual field, and a full field in the left visual field. By introducing a fixation subsystem with a $\pm 10°$ field, based on a TI DLP4500 display, using a pellicle we could provide a moveable fixation point as well as a visual stimulus. Image quality was good over most of the imaging range. Figure 5 shows results from a simple montage generated by serially displacing the steering mirrors across the field from -13° to +10° with a second row generated by displacing the imaging field vertically by roughly 1°. To montage images required only lateral and vertical displacements. In our previous wide field system[20] there was field distortion which required rotating sub images based on their location within the field. While there can still be slight physiological cyclo-rotations of the eye, the system greatly improves the fidelity and should be more amenable to eye tracking strategies since the displacements remain essentially orthogonal over the imaging field. Image quality was also good over most of the field. The inset figures of Figure 5 show the images acquired four locations across the

Figure 4. Schematic of short wavelength detection. A single beam from the retina is sent to three detectors simultaneously. The PSF is separated into directly backscattered light by a pinhole at the retinal conjugate plane. The surrounds of the PSF (multiply scattered light) is re-imaged onto a digital micromirror device (DMD), which diverts it to one of two detectors. The pattern shown is a half annulus, oriented horizontally.

measured field. Only in the most nasal retinal location does image quality decrease a bit, and it is not clear if this is a failure of the aberration control, or decreased image quality arising from the very thick overlying nerve fiber layer in this region, which is adjacent to the optic nerve head. This decrement was not visible in all subjects, but modeling suggests that control should be adequate here, however the system isoplanatism is decreased in hyperopes and at increasing angles from the optic axis of the system.

The imaging has also proven to be efficient. The entire cone mosaic shown below (Figure 5A), required only about 12 minutes for this 22°x3° strip, although this patient had good fixation. our standard imaging protocol in controls and subjects with retinal disease, takes on the order of 35 minutes to obtain two focal planes for two regions: 1) 6°x6° foveal centered and 2) a 3°x8° strip of the temporal retina.
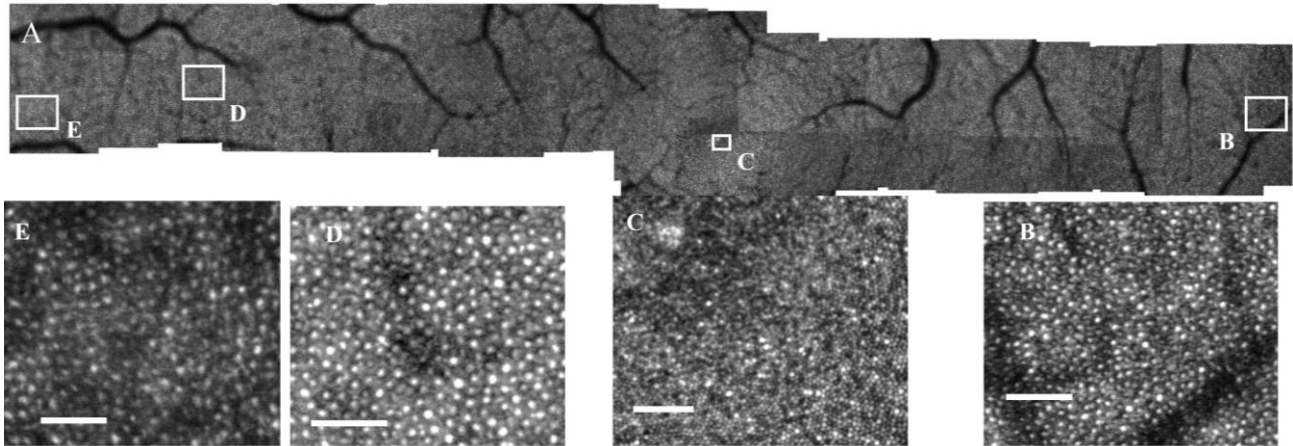

Figure 5. Example of beam steering system used to image cones in an undilated 34 yo male. Images were collected as averages of 100 frames video. After each video sequence the system displaced the beam by 1°, and acquired the next, generating a 22°x3° montage (A). Image quality is good into the temporal retina out to 10° (B), and in the foveal center (C), as well as at 10° in the nasal retina. Image quality decreases somewhat at the edge of the steering field (E- 12° nasal). Scale bars 50 μm.
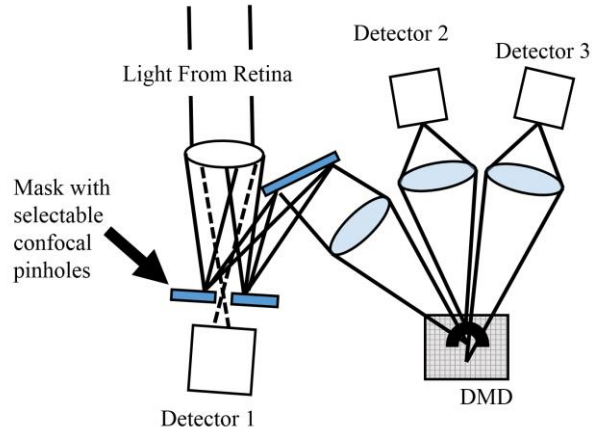
3.3 Flexible Detection and Temporal Offset imaging.

When a small confocal aperture is used, light that is multiply scattered is primarily imaged outside the aperture and thus falls on the reflective surface of the confocal mask. This light was directed into the second arm of the short wavelength detection system and re-imaged onto the surface of the DMD. This light generated excellent quality multiply scattered light images with small artifacts arising from the same-side resets of the mirror segments. We confirmed that by programming appropriate shapes onto the DMD we could control selectivity for different aspects of the retinal image. This was particularly striking for oriented retinal features, and thus we could selectively enhance individual retinal features by changing the orientation of programmable masks. However, we also determined that a fixed half annulus capturing light from approximately 8 Airy disc (AD) diameters to 23 AD, and directing the rest of the multiply scattered light to the other detector provided relatively good contrast of retinal vessels. An example for a diabetic eye is shown in Figure 6. Here we see images from a single 100 frame (~3.3 s) acquisition, focused on the inner retina. The confocal image (A) shows high contrast details of the vessel surface. The offset aperture image from the longer wavelength channel (B) shows vessel walls and an area of mild edema (top center). The
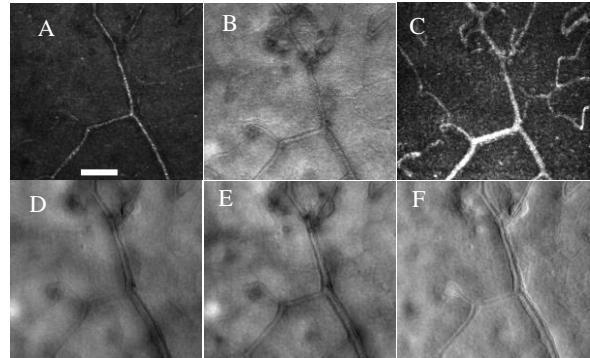

Figure 6. Images of a diabetic retinal showing images from all four detectors, from a single 100 frame acquisition. A: Confocal image, B: Offset Aperture Image from long wavelength channel, C: Flow map from variance of offset image D: Image obtained with a half annular aperture programmed onto the DMD. , E: complement (rest of light) that is not directed to D or A. F: Contrast between D and E (D-E)/(D+E). Scale bar 100 μm.

DMD channels (D and E) show the same features, but the contrast image (F) shows vessel walls very clearly making quantification much simpler. Similarly, computing the time variance of the offset channel image provides high quality maps of vessels.

By changing the short wavelength aperture to a 10X Airy disc diameter and offsetting it we can also use the system to make blood flow measurements, providing a temporal delay between the channels[14].

4. CONCLUSIONS

Adaptive Optics for retinal imaging is becoming increasingly common. Recent advances in both system design and system control are making it robust enough for routine measurements in patients.

5. ACKNOWLEDGEMENTS

6. REFERENCES CITED

[1] Bedggood, P., Daaboul, M., Ashman, R. *et al.*, "Characteristics of the human isoplanatic patch and implications for adaptive optics retinal imaging," Journal of Biomedical Optics, 13(2), (2008).

[2] Bedggood, P. A., Ashman, R., Smith, G. *et al.*, "Multiconjugate adaptive optics applied to an anatomically accurate human eye model," Optics Express, 14(18), 8019-8030 (2006).

[3] Thaung, J., Knutsson, P., Popovic, Z. *et al.*, "Dual-conjugate adaptive optics for wide-field high-resolution retinal imaging," Optics Express, 17(6), 4454-4467 (2009).

[4] Elsner, A. E., Burns, S. A., Weiter, J. J. *et al.*, "Infrared imaging of sub-retinal structures in the human ocular fundus," Vision Research, 36(1), 191-205 (1996).

[5] Elsner, A. E., Dreher, A., Beausencourt, E. *et al.*, "Multiply scattered light tomography:vertical cavity surface emitting laser array used for imaging subretinal structures," Lasers and Light in Ophthalmology, 8, 193-202 (1998).

[6]   Elsner, A. E., Miura, M., Burns, S. A. *et al.*, "Multiply scattered light tomography and confocal imaging: detecting neovascularization in age-related macular degeneration," Optics Express, 7(2), 95-106 (2000).

[7]   Burns, S. A., Elsner, A. E., Mellem-Kairala, M. B. *et al.*, "Improved contrast of subretinal structures using polarization analysis," Investigative Ophthalmology & Visual Science, 44(9), 4061-4068 (2003).

[8]   Chui, T. Y. P., VanNasdale, D. A., and Burns, S. A., "The use of forward scatter to improve retinal vascular imaging with an adaptive optics scanning laser ophthalmoscope," Biomedical Optics Express, 3(10), 2537-2549 (2012).

[9]   Scoles, D., Sulai, Y. N., and Dubra, A., "In vivo dark-field imaging of the retinal pigment epithelium cell mosaic," Biomedical Optics Express, 4(9), 1710-1723 (2013).

[10]   Burns, S. A., Elsner, A. E., Chui, T. Y. *et al.*, "In vivo adaptive optics microvascular imaging in diabetic patients without clinically severe diabetic retinopathy," Biomedical Optics Express, 5(3), 961-974 (2014).

[11]   Chui, T. Y. P., Gast, T. J., and Burns, S. A., "Imaging of Vascular Wall Fine Structure in the Human Retina Using Adaptive Optics Scanning Laser Ophthalmoscopy," Investigative Ophthalmology & Visual Science, 54(10), 7115-7124 (2013).

[12]   Sulai, Y. N., Scoles, D., Harvey, Z. *et al.*, "Visualization of retinal vascular structure and perfusion with a nonconfocal adaptive optics scanning light ophthalmoscope," Journal of the Optical Society of America A, 31(3), 569-579 (2014).

[13]   Burns, S. A., De Castro, A., Sawides, L. *et al.*, "A Programmable Aperture Adaptive Optics SLO," Investigative Ophthalmology & Visual Science, 57(12), (2016).

[14]   de Castro, A., Huang, G., Sawides, L. *et al.*, "Rapid high resolution imaging with a dual-channel scanning technique," Opt Lett, 41(8), 1881-4 (2016).

[15]   Zou, W. Y., Qi, X. F., Huang, G. *et al.*, "Improving wavefront boundary condition for in vivo high resolution adaptive optics ophthalmic imaging," Biomedical Optics Express, 2(12), 3309-3320 (2011).

[16]   de Castro, A., Sawides, L., Qi, X. F. *et al.*, "Adaptive optics retinal imaging with automatic detection of the pupil and its boundary in real time using Shack-Hartmann images," Applied Optics, 56(24), 6748-6754 (2017).

[17]   Burns, S. A., Wu, S., Delori, F. *et al.*, "Direct Measurement Of Human-Cone-Photoreceptor Alignment," Journal of the Optical Society of America a-Optics Image Science and Vision, 12(10), 2329-2338 (1995).

[18]   Prieto, P. M., Vargas-Martin, F., Goelz, S. *et al.*, "Analysis of the performance of the Hartmann-Shack sensor in the human eye," Journal of the Optical Society of America A-Optics Image Science and Vision, 17(8), 1388-1398 (2000).

[19]   Burns, S. A., Tumbar, R., Elsner, A. E. *et al.*, "Large-field-of-view, modular, stabilized, adaptive-optics-based scanning laser ophthalmoscope," J Opt Soc Am A Opt Image Sci Vis, 24(5), 1313-26 (2007).

[20]   Ferguson, R. D., Zhong, Z. Y., Hammer, D. X. *et al.*, "Adaptive optics scanning laser ophthalmoscope with integrated wide-field retinal imaging and tracking," Journal of the Optical Society of America a-Optics Image Science and Vision, 27(11), A265-A277 (2010).

[21]   Webb, R. H., Hughes, G. W., and Delori, F. C., "Confocal scanning laser ophthalmoscope," Applied Optics, 26, 1492-1499 (1987).

[22]   Dubra, A., and Sulai, Y. N., "First-order design of a reflective viewfinder for adaptive optics ophthalmoscopy," Optics Express, 20(24), 26596-26605 (2012).